Fourth International Symposium on Marine Propulsors
smp'15, Austin, Texas, USA, June 2015

Validation of a Propeller Model for Maneuvering Applications

J. Ezequiel Martin[1,*], Alireza Mofidi[1], Thad Michael[2], Pablo M. Carrica[1]

[1] IIHR-Hydroscience and Engineering, The University of Iowa, Iowa City, IA 52242, USA
[2]Naval Surface Warfare Center Carderock Division, West Bethesda, MD 20817,USA
*corresponding author: juan-martin@uiowa.edu, 1-319-335-6022

ABSTRACT

Two modeling strategies for propellers are presented and validated. Experimental data for a propeller in oblique flow is compared to numerical results obtained from the unsteady Reynolds averaged Navier-Stokes solver CFDShip-Iowa v4.5 with the complete geometry of the propeller represented and for the solver coupled with the vortex lattice lifting surface method PUF-14. Validation in oblique conditions is relevant to maneuvering applications where propellers regularly encounter incoming flow with an important lateral component. Results show that fully discretized blades reproduce the experimental data very well, while the coupled model reproduces the mean propulsion parameters well, but fails to fully represent higher harmonics components of the force signal. Reasons for the discrepancy between the two methods are analyzed.

Keywords

Computational Fluid Dynamics; Vortex Lattice Methods

1 INTRODUCTION

High resolution simulation of maneuvers for both surface ships and submarines presents unique difficulties, due to the disparity between the relatively long maneuver time and the small time step required to accurately capture the propeller rotation. It is not uncommon for such simulations to require tens to hundreds of thousands of time steps for completion. This limits the applicability of fully discretized propeller simulations for maneuvering to research projects, for which turnaround time is not as stringent as for design and production applications.

If a model, rather than the true geometry of the propeller, is considered, simulation time can be shortened, typically by an order of magnitude. Many propeller models are available from simple non-interacting body forces models such as the Hough and Ordway (1965) model to more complex potential flow solvers based on vortex lattice (VLM, Warren *et al.*, 2000) and panel (Kerwin *et al.*, 1987) lifting surface methods. While the performance of these models is usually acceptable for steady conditions, more rigorous testing is required to verify their applicability to the highly unsteady conditions that are found during maneuvering. As an intermediate condition for testing these models between the idealized conditions presented by an open water curve experiment and the unsteady conditions observed during maneuvering of a self-propelled vessel, open water curves in oblique flow are considered. While other unsteady features, for instance wakes from appendages placed upstream of the propeller (Martin *et al.*, 2014; Chase and Carrica, 2013) can have an important effect on the propeller operation, arguably the existence of a relative angle between the advance direction and the propeller axis and the non-uniformity of the incoming velocity profile can have the most prominent effect on the propeller operation during a maneuver. Either of these two conditions can be approximated as quasi-steady during a maneuver as changes occur much slower than the typical time necessary for the propeller to adjust to the new configuration, and therefore the study of oblique or non-uniform incoming conditions are of interest to quantify the model performance.

We present the implemented tight coupling between a computational fluid dynamics code CFDShip-Iowa v4.5 and a vortex lattice lifting-surface solver (PUF-14), and review previous results for a stock propeller (Martin et al., 2014). New open water curve (OWC) results for a propeller in oblique flow with both rotating, discretized blades and using PUF-14 are compared with experimental results from Boswell *et al.* (1981).

2 FORMULATION

2.1 Approach

The computations are performed with the ship hydrodynamics code CFDShip-Iowa v4.5 that solves the RANS/DES equations using a blended k–ε/k–ω turbulence model. The domain is discretized using multiblock/overset structured grids with fully dynamic overset capabilities to enable motions. Several controllers and auto-pilot models enable full maneuvering and self-propulsion capabilities. Numerical methods include finite difference discretization, with a second- to fourth-order upwind-biased discretization of the convection terms and a second-order centered scheme for the viscous terms. The temporal terms are discretized

using a second-order backwards Euler scheme. Incompressibility is enforced by a strong pressure/velocity coupling, and achieved using a projection algorithm. A brief description of the equations solved is presented below; further details are described in Carrica et al. (2007) and the literature therein.

CFDShip-Iowa v4.5 solves the incompressible Navier-Stokes equations in an inertial coordinate system. Mass and momentum equations are:

$$\frac{\partial u_j}{\partial x_j} = 0 \tag{1}$$

$$\frac{\partial u_i}{\partial t} + \frac{\partial u_i u_j}{\partial x_j} = -\frac{\partial p}{\partial x_i} + \frac{\partial}{\partial x_j}\left[\frac{1}{\mathrm{Re}_{eff}}\left(\frac{\partial u_i}{\partial x_j} + \frac{\partial u_j}{\partial x_i}\right)\right] + s_i \tag{2}$$

where S_i is the body force provided by the coupled propeller solver, if present. Equations are non-dimensionalized with an arbitrary nominal velocity, U_0, and reference length, L_0, in this case the propeller radius. The dimensionless piezometric pressure is defined as $p = P / \rho U_0^2 + 2k/3$ with P the pressure with respect to atmospheric, and $1/\mathrm{Re}_{eff} = 1/\mathrm{Re} + \nu_t$ is the effective Reynolds number with ν_t the turbulent viscosity obtained from a turbulence model.

The turbulence is modeled using a blended $k-\varepsilon / k-\omega$ model (Menter, 1994), where the turbulent kinetic energy, k, and the specific dissipation rate, ω, are computed from

$$\frac{\partial k}{\partial t} + \left(u_j - \sigma_k \frac{\partial \nu_t}{\partial x_j}\right)\frac{\partial k}{\partial x_j} - \frac{1}{P_k}\frac{\partial^2 k}{\partial x_j^2} + s_k = 0 \tag{3}$$

$$\frac{\partial \omega}{\partial t} + \left(u_j - \sigma_\omega \frac{\partial \nu_t}{\partial x_j}\right)\frac{\partial \omega}{\partial x_j} - \frac{1}{P_\omega}\frac{\partial^2 \omega}{\partial x_j^2} + s_\omega = 0 \tag{4}$$

with turbulent viscosity and effective Peclet numbers defined as

$$\nu_t = \frac{k}{\omega},\ P_k = \frac{1}{1/\mathrm{Re} + \sigma_k \nu_t},\ P_\omega = \frac{1}{1/\mathrm{Re} + \sigma_\omega \nu_t} \tag{5}$$

where $s_k = -G + \beta^* \omega k$ and $s_\omega = \omega\left(\beta^* \omega - \gamma G/k\right) - 2\left(1-F_1\right)\sigma_{w2}\left(\partial k/\partial x_j\, \partial \omega/\partial x_j\right)/\omega$ are the sources for k and ω respectively, and $G = \nu_t \tau_{ij} \partial u_i/\partial x_j$ the kinetic energy production. The blending function F_1 switches between the $k-\omega$ model near the wall to the $k-\varepsilon$ model on the free-stream region.

The current version of CFDShip-Iowa v4.5 includes an optional coupling implementation of PUF-14, which can be run on its own processor in concurrent (lagged) or sequential mode. PUF-14 has execution times comparable to those of CFDShip-Iowa v4.5, resulting in a considerable increase in computation time per time step when using sequential mode. The lagged mode introduces virtually no increase in execution time, while still producing accurate results. Overall the concurrent CFDShip-Iowa v4.5/PUF-14 coupled approach reduced the computational time by a factor of about seven (Martin *et al.*, 2014; Chase and Carrica, 2013).

PUF-14 was designed for coupled operation with a CFD solver. Wake and blade location velocities from the CFD code are used to update the effective velocities used as inflow for the vortex lattice solution. The model includes modelling of blade thickness via sources at the vortex lattice control points, hub modelling by vortex images, and an explicitly shed wake also described using a vortex lattice. The wake position and geometry is updated at each time step using the CFD velocity to convect thewake geometry of the previous time step. Incoming flow and rotation rate are also updated at each time step. Finally, the computed blade solution is used to compute the local force on the fluid, as well as the force on the shaft, and these are returned to the CFD solver, to be use respectively in the solution of the fluid equations and the six-degrees-of-freedom equations for the propelled body.

3 RESULTS AND DISCUSSION

3.1 Previous Results – Mercury Vengeance Stock Propeller

Figure 1a shows the OWC efficiency curve for a Mercury Vengeance stock propeller. This propeller was used to propel the research underwater vehicle ONR Body 1 (Martin *et al.*, 2014), but no OWC curves were measured during the experimental campaign. In order to successfully complete the simulation of those maneuvers, adjustment of the drag coefficient in PUF-14 was required to match the results obtained for the discretized geometry; this is particularly important for model scale experiments where viscous effects must be considered. The friction coefficient for the blade (Figure 1b) shows that the chosen value for $Re_{\mathrm{prop}}=10^5$ (approximately the value used in the experimental setup) matches well with the predicted value from the discretized simulation.

The presented data shows that under these conditions, coupling the VLM solver with a URANS CFD solver can produce accurate propeller coefficients.

3.2 P4661 Propeller

There are few examples of experimental propeller measurements at oblique advance angles. The data in Boswell *et al.* (1981) presents a complete analysis of the blade loading of different propellers at inclined shaft angles. The data for propeller P4661 is compared here to numerical results, as it is the most complete set of those reported by Boswell *et al.* (1981). The actual base OWC is not reported therein, but can be found in Black and Michael (2003) with the geometry of the propeller. In the work presented here, a right-handed version of the propeller has been used for computations. The results have been adjusted for comparison with the left-handed propeller used for the

measurements where required. Experimental results were reported using a different definition of the advance velocity U_A and were interpolated when necessary for comparison to current results; whenever experimental was interpolated, it is clearly indicated in the text. Additionally, simulations were computed at a Reynolds number higher, by a factor 2, with respect to experimental values.

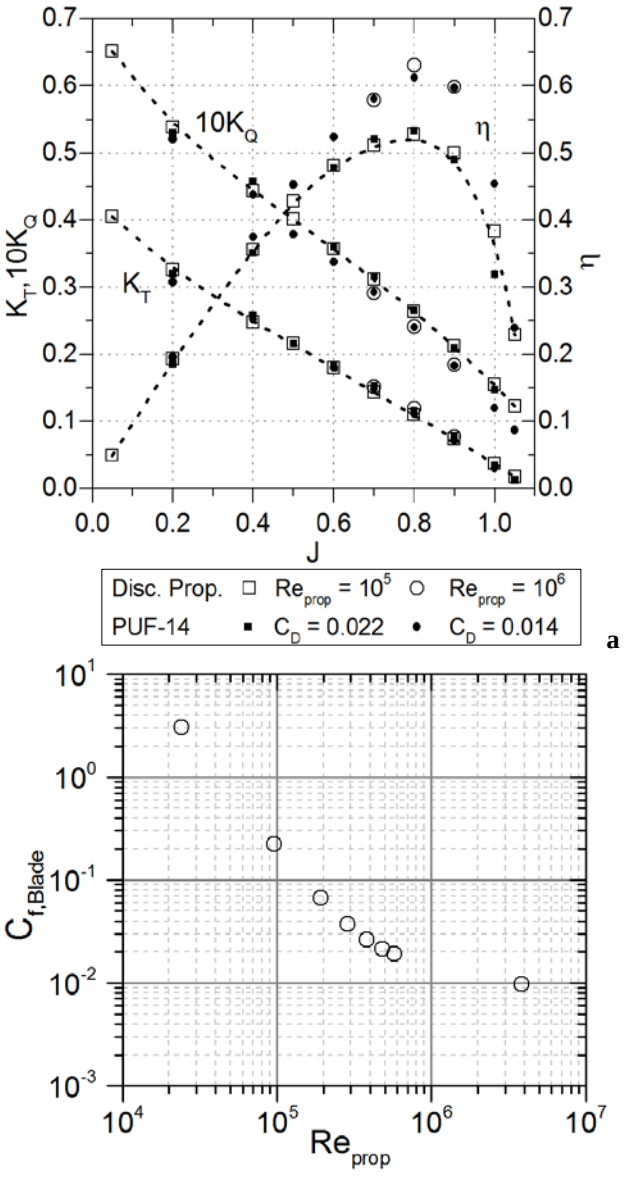

Figure 1: (a) Open water efficiency curves for Vengeance propeller. Calculations for discretized blades are shown with open symbols (squares correspond to $\mathbf{Re_{prop}} = 5x10^5$, circles to $\mathbf{Re_{prop}} = 5x10^6$). Results for the coupled code are shown as solid symbols (circles correspond to $\mathbf{C_d} = 0.014$, squares to $\mathbf{C_d} = 0.0225$); Dashed lines for K_T and K_Q correspond to a cubic best-fit for the low Reynolds discretized blade data, while the efficiency curve is obtained from those and Eq. (1). (b) Friction coefficients for discretized blades, as a function of the propeller Reynolds number, based on chord at 0.7R

Boswell *et al.* (1981) performed experiments with the 4661 propeller in a towing with an apparatus that allowed the propeller shaft to be inclined relative to the inflow. They mounted the propeller on the end of a shaft driven from downstream and data was collected at 0, 10, 20 and 30 degrees of shaft inclination. They measured the periodic single-blade loads and compared the results to lifting surface models available at the time of the study.

Figure 2 shows the overset surface grid defining the shaft and blades geometry, used for the discretized calculation. A static overset interpolation was used, by pre-calculating the interpolation coefficients and simulating the propeller rotation by solid body rotation. An inlet velocity was imposed for both the x- and y-components, thus creating the oblique incoming flow to the propeller. The static interpolation represents an important reduction in computational requirements as the overset connectivity calculation is resource-intensive. A very large (about 100 propeller diameters) background grid was used to ensure that the boundaries of the system did not affect the results. Such a large domain is not usually necessary for this type of computations, but it is important here as lateral velocities can be significant and the forward motion of the system is simulated by imposing incoming flow velocities at the boundary. Table 1 summarizes the dimensions of the grids used. The difference in number of grid points used is another advantage of the coupled method, as not only the blade grids are eliminated, but also a much coarser wake refinement is used, since it is no longer possible to resolve tip vortices. The coordinate system used in measuring the experimental forces and to report the current results is shown in Figure 2. A total of 20 different conditions were simulated, at different angles and five different advance coefficients, for the two modelling approaches.

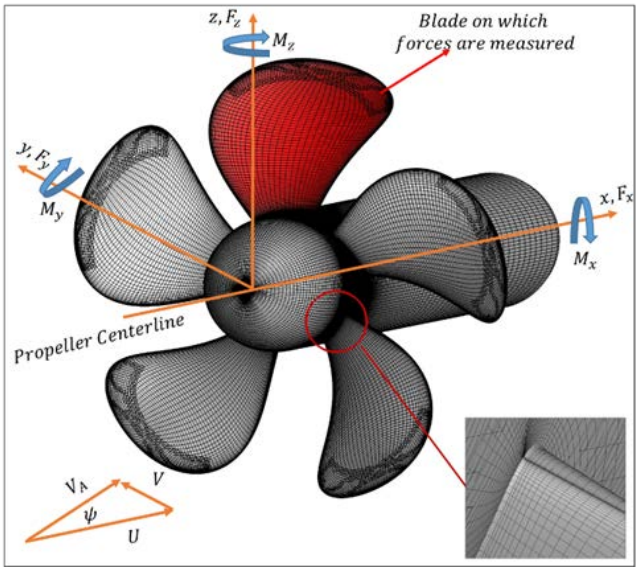

Figure 2: Domain and coordinates convention for propeller P4661 open water simulations.

The general characteristics of the CFD solutions are shown in Figures 3 and 4. Figure 3 shows the results for both coupled and discretized computations at 0 and 30 degrees at the design advance coefficient (J = 1.14). Figure 4 shows the same incoming flow conditions for the highest loading condition simulated (J = 0.6). Due to the different inherent characteristics of the two methods, many vortical signatures present in the discretized calculation are missing from the coupled one. For straight ahead conditions (left column in Fig. 3) the agreement between the two codes, with respect to the induced velocities in the wake is extremely good. At 30 degrees, while the overall distribution of velocities is similar, the coupled method under-predicts the velocity in regions exposed to the lateral velocity and over-predicts the speed behind the shaft. A similar pattern is observed at high load conditions, with the additional appearance of an unrealistic recirculation bubble near the propeller region for the coupled solver.

Table 1: Grid system for propeller P4661 with direct (D) or coupled (C) simulation of the blades.

Grid	Size	Total Points	Grid Type	Model
Shaft	181x51x121	1.12M	'O'	D/C
Blades	5x121x46x101	5x563K	'O'	D. only
Blades Tips	5x61x51x61	5x190 K	Wrapped	D. only
Ref. Wake	201x241x241	11.7M	Cartesian	D. only
Ref.PUF	181x51x61	563K	Cylindrical	C. only
Background	121x95x95	1.09 M	Cartesian	D/C
Total D.		**17.7 M**		
Total C.		**2.8 M**		

The direct method matches the experimental results well over the range of advance coefficients, while the coupled results match reasonably well near the design advance coefficient, but over-predicts at high J values, and under-predicts at high loads. This characteristic of lifting surface models have been previously described (Black and Michael, 2003), and it has been attributed to the limitations of the model in capturing wake roll up and leading edge separation.

The calculated OWCs for the two methods intersect at $J \sim 1.0$ for straight ahead conditions. The intersection point moves towards higher J values as the incidence angle increases. Interestingly, near the design point, the overall effect of the propeller is better matched between the two models at a high incident angle, as shown in Figure 5, even though the induced wake velocity distribution presents important differences. At low advance ratios, the coupled model under-predicts both thrust and torque, which can differ by 10 to 15 percent between the two models for all angles considered.

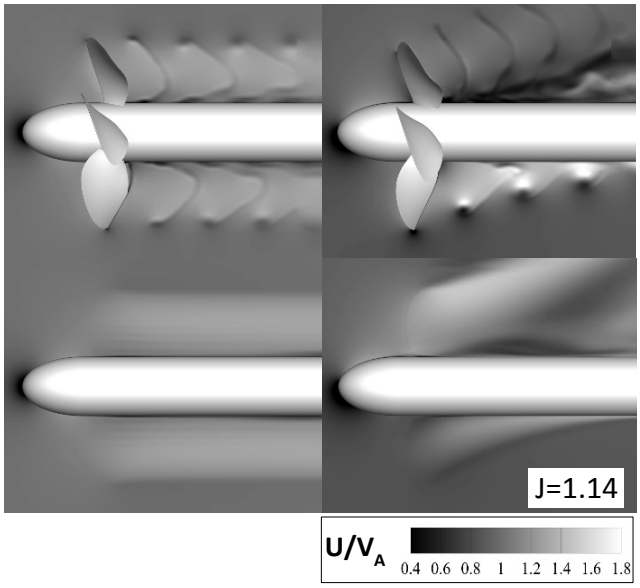

Figure 3: Longitudinal fluid velocity at advance coefficient J = 1.14 (design value). Top: discretized blades; bottom PUF-14 modelled propeller. Shaft angle is zero for left column and30 degrees for right column plots. Velocity is non-dimensionalized with carriage advance velocity.

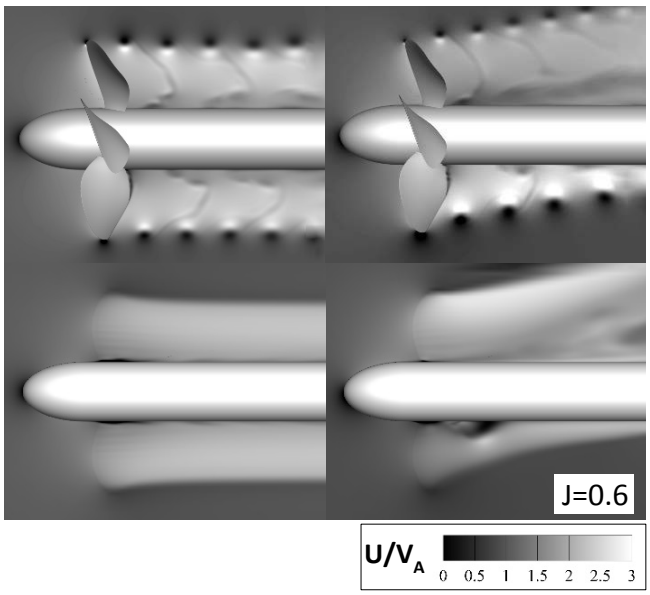

Figure 4: Longitudinal fluid velocity at advance coefficient J = 0.6. Top: discretized blades; bottom PUF-14 modelled propeller. Shaft angle is zero for left column and 30 degrees for right column plots. Velocity is non-dimensionalized with carriage advance velocity.

The calculated OWCs for the two methods intersect at $J \sim 1.0$ for straight ahead conditions. The intersection point moves towards higher J values as the incidence angle increases. Interestingly, near the design point, the overall effect of the propeller is better matched between the two models at a high

incident angle, as shown in Figure 5, even though the induced wake velocity distribution presents important differences. At low advance ratios, the coupled model under-predicts both thrust and torque, which can differ by 10 to 15 percent between the two models for all angles considered.

Figure 5 compares the calculated OWCs for the two methods at 0 and 30 degrees. Experimental data for 0 degrees are also included. OWCs for all simulated angles are presented in Figures 6 and 7, for direct and coupled simulations, respectively. The standard definitions for thrust, K_T, and torque, K_Q, coefficient were used, as well as for propeller efficiency, η:

$$K_T = \frac{F_x}{\rho n^2 D^4}; K_Q = \frac{M_x}{\rho n^2 D^5}; \eta = \frac{J K_T}{2\pi K_Q}, \qquad (6)$$

where ρ is the fluid density, n the propeller rotational speed, D the propeller diameter, F_x and M_x are the longitudinal propeller thrust and torque, respectively, and J is the advance ratio, defined as $J = U_A(nD)^{-1}$, with U_A the advance speed of the carriage.

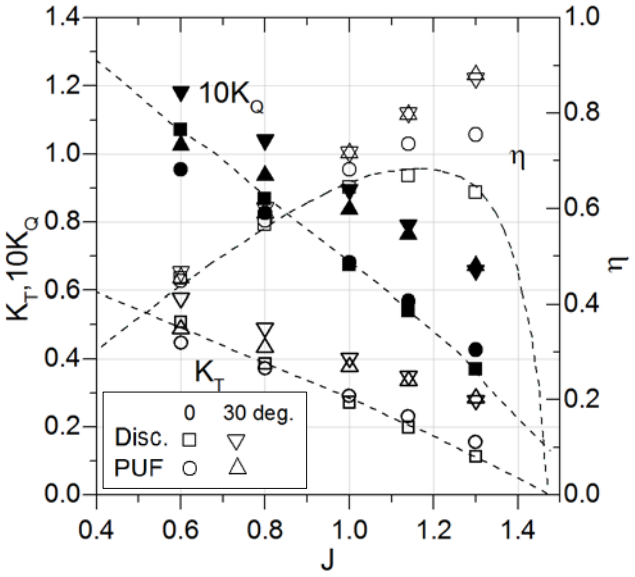

Figure 5: Open water curves for propeller P4661 at 0 and 30 degree shaft angles with respect to the carriage advance direction. Discretized geometry and coupled model results are shown. Dotted lines correspond to experimental values at 0 degrees. Solid symbols correspond to K_Q, thick line symbols to K_T and thin line symbols to efficiency. The model used and shaft angle are described in the plot legend.

Figures 6 and 7 show the complete OWCs for the two methods. The overall effect of the inclined shaft, in terms of the OWCs is to increase the loading of the blade and the efficiency of the propeller. Even though the normal velocity to the propeller decreases as the shaft angle increases with respect to the incoming flow, for constant carriage velocity, this effect can only partially explain the increase in efficiency observed. More importantly, the flow conditions for the blade result in largely variable angle of attack at different radial positions, and consequently different loading on the blade. Conditions are such that for certain low loading conditions, the blade behaves a turbine, rather than a propeller during part of the rotation.

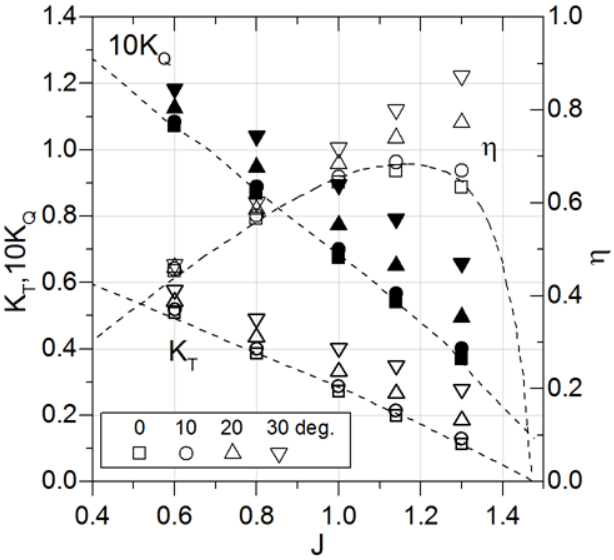

Figure 6: Open water curves for propeller P4661 at different shaft angles with respect to the carriage advance direction. Blades simulated using discretized geometry. Dotted lines correspond to experimental values at 0 degree. Solid symbols correspond to K_Q, thick line symbols to K_T and thin line symbols to η. The shaft angle is described in the plot legend.

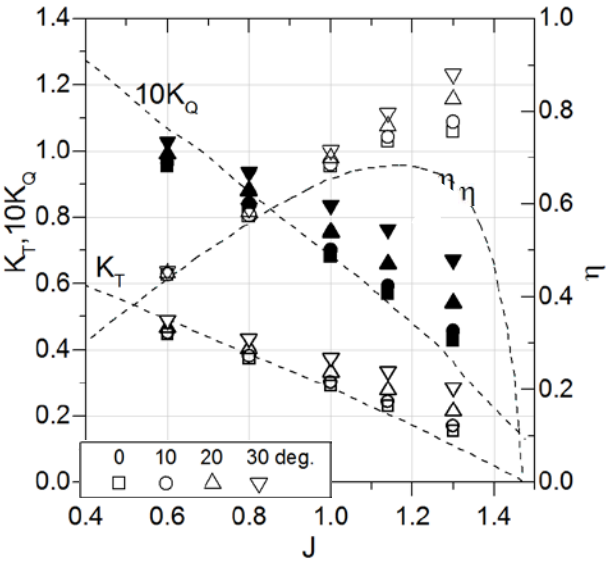

Figure 7: Open water curves for propeller P4661 at different shaft angles with respect to the carriage advance direction. Blades simulated using PUF-14 model. Dotted lines correspond to experimental values at 0 degrees. Solid symbols correspond to K_Q, thick line symbols to K_T and thin line symbols to η. The shaft angle is described in the plot legend.

Figures 8 through 11 present the temporal evolution of the integrated force over the blade, for both modeling methods at high and low loading conditions. As discussed previously, mean values differ between the two methods by less than 15 percent; however, differences in fluctuations are much more important, with the direct method accounting for up to 40% larger peak values. Following Boswell *et al.* (1981) notation, the total force, expressed as a thrust coefficient can be decomposed as

$$K_{\mathrm{Fx}}(\theta) = \overline{K_{\mathrm{Fx}}} + \sum_{i=1,N} K_{\mathrm{Fx,i}} \cos\left(i\theta - \phi_{\mathrm{Fx,i}}\right) \qquad (7)$$

with $K_{\mathrm{Fx,i}}$ the amplitude of the i^{th} harmonic, and $\phi_{\mathrm{Fx,i}}$ its phase. For most conditions, the first harmonic is largely dominant, and only at large angles and advance coefficients the second harmonic contribution is also needed to accurately represent the total blade force. A similar decomposition is possible for lateral forces and moments. Comparison of the results between the two methods shows that the resulting phase varies considerably for the coupled method, as evidenced by the shift in angle position of the minima in F_x and F_y while little change is observed for the direct method, which is consistent with reported behaviour for the experimental dataset.

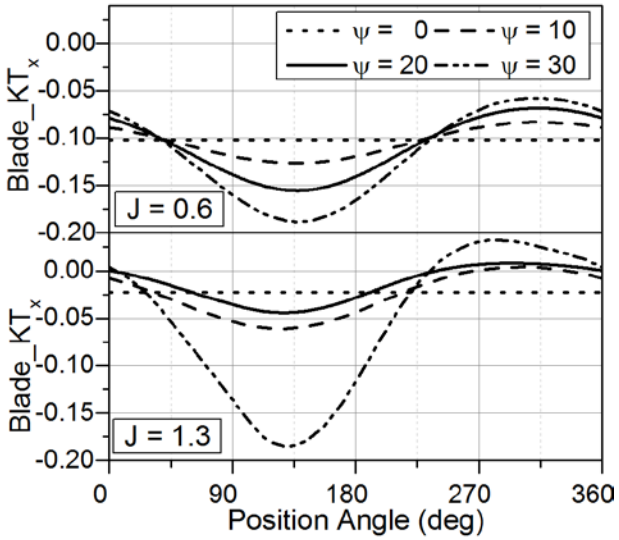

Figure 8: Longitudinal blade forces, expressed as a K_T coefficient as a function of blade position, for discretized geometry, at different shaft angles. Top panel J = 0.6; lower panel J = 1.3.

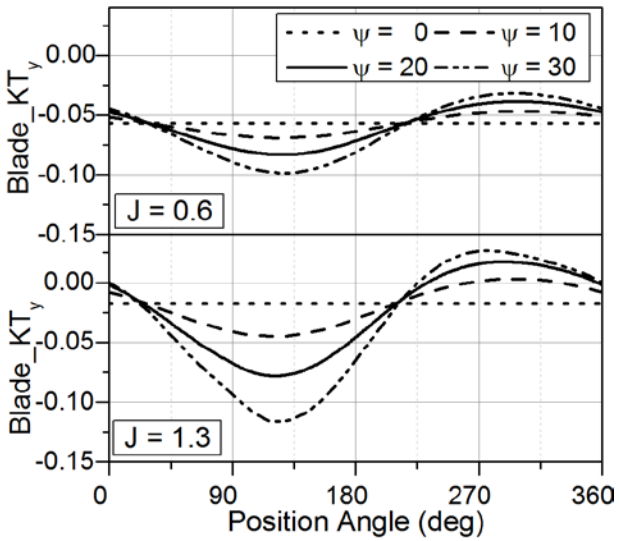

Figure 9: Lateral (y) blade forces, expressed as a K_T coefficient as a function of blade position, for discretized geometry, at different shaft angles. Top panel J = 0.6; lower panel J = 1.3.

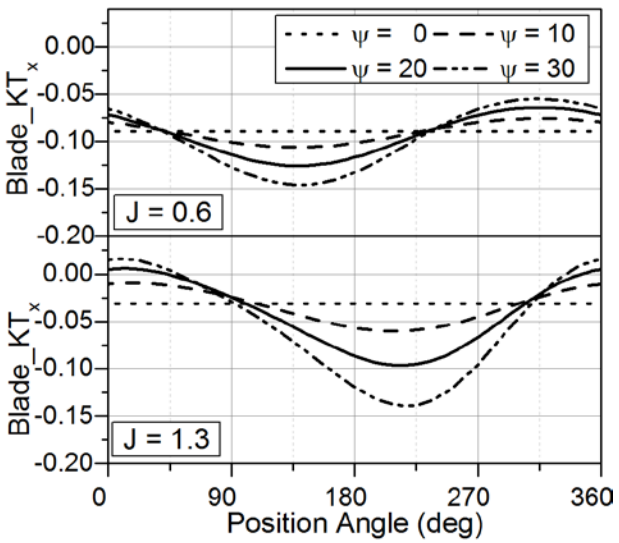

Figure 10: Longitudinal blade forces expressed as a K_T coefficient as a function of blade position, for PUF-14 modelled propeller, at different shaft angles. Top panel J = 0.6; lower panel J = 1.3.

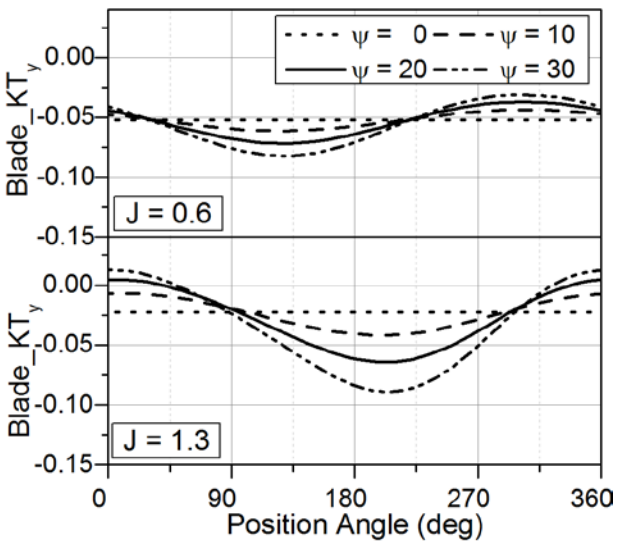

Figure 11: Lateral (y) blade forces, expressed as a K_T coefficient as a function of blade position, for PUF-14 modelled propeller, at different shaft angles. Top panel J = 0.6; lower panel J = 1.3.

Figure 12 summarizes the complete dataset of first harmonic amplitudes of the longitudinal force. A non-dimensionalization similar to, but different from Boswell *et al.* (1981) was followed,

$$K_{\mathrm{Fx,i}} = \frac{F_{x,i}}{\rho n U_A D^3} \tag{8}$$

instead of the standard non-dimensionalization presented in Eq. (6). Note that U_A is the carriage speed, while Boswell *et al.* (1981) uses V_A, the volume mean wake in the shaft longitudinal direction from a wake survey. U_A is also used in the definition of J in this paper instead of V_A. This difference has been accounted for when plotting the experimental results.

In Figure 12, the discrepancy between the experimental results and the direct propeller model results reaches a maximum of about 20% of the experimental values, with an average error of about 11%, while much larger errors are found for the coupled model, with an average error of 25% and a maximum one of 37%.

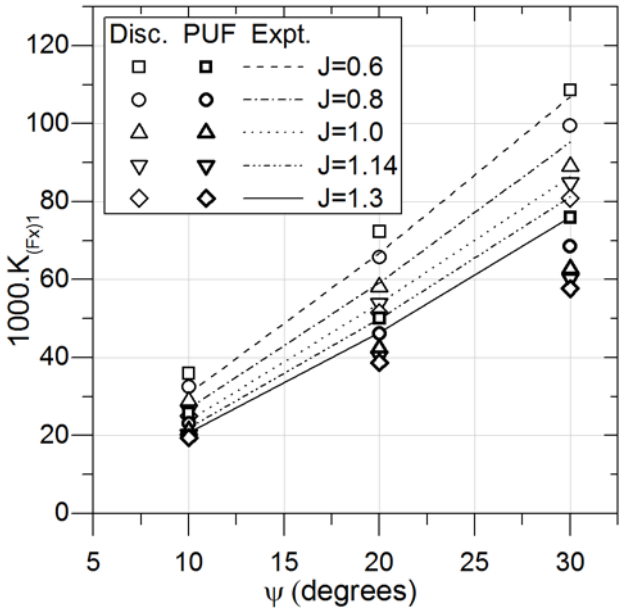

Figure 12: Amplitude of the first harmonic for propeller P4661 at different shaft angles with respect to the carriage advance direction. Blades simulated using PUF-14 model. Lines correspond to experimental values, and symbols to discretized or modelled blades as shown in plot legend. Experimental values are interpolated (and for J=0.6. extrapolated) to reconcile the different definitions of the advance velocity between experiments and simulations.

Figures 13 and 14 represent the first harmonics amplitude a as function of the advance ratio for constant shaft inclination angle. Quantities are reported as a ratio to the value at the design advance coefficient, following Boswell *et al.* (1981). Consistently fair agreement between the experimental results and the direct simulation values is observed for the forces and moments reported. Coupled results are not shown for clarity, but present typical errors similar to those previously described.

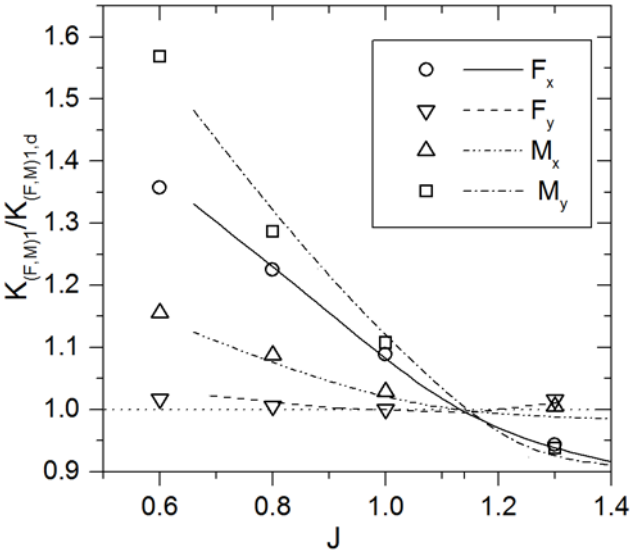

Figure 13: Amplitude of the first harmonic as a fraction of the value near design J for longitudinal and lateral forces and moments for direct method at shaft angle 10 degrees. Lines correspond to experimental values from Boswell *et al.* (1981) and symbols to direct method simulations.

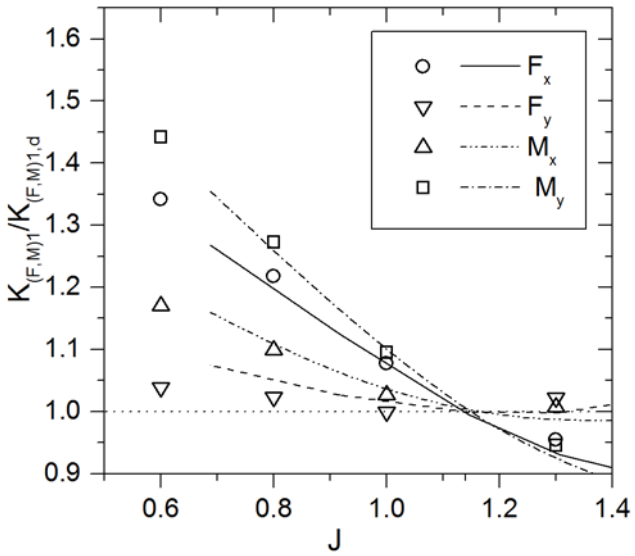

Figure 14: Amplitude of the first harmonic as a fraction of the value near design J for longitudinal and lateral forces and moments for direct method at shaft angle 20 degrees. Lines correspond to experimental values from Boswell *et al.* (1981) and symbols to direct method simulations.

4 CONCLUSIONS AND FUTURE WORK

Exhaustive simulations of a propeller in oblique incoming flow conditions were performed, using two different

representations of the propeller. Both methods have been previously shown to be able to reproduce the propulsion of free bodies over prescribed maneuvers. The purpose of the present work was to quantify under more controlled conditions the performance and limitations of both methods for conditions where the flow is not aligned with the propeller, a situation commonly encountered during maneuvers.

Results for the discretized blade representation, or direct modelling approach, yield excellent agreement with the available experimental measurements, over a range of advance ratios and shaft incline angles. The second approach, for which a vortex lattice method was coupled to the CFD solver, generated average forces in fair agreement with the experimental values, but under-predicted higher harmonics by up to 40%. Previous results for a similar implementation of PUF-14 coupled to a CFD solver, by Black and Michael (2003), are in better agreement with the experimental data, and the possibility of an error in the current implementation is being examined.

ACKNOWLEDGMENTS

This research was supported by the US Office of Naval Research under grants N000141110232 and N0001413AF00002, with Dr. Ki-Han Kim as the program manager. The computations were performed on University of Iowa High Performance Computing clusters Helium and Neon.

REFERENCES

Black, S.D., Michael, T.J. (2003), "Experiences using a Coupled Viscous/Potential-Flow Unsteady Propeller Analysis Procedure," SNAME Propellers/Shafting Symp., Virginia Beach, VA.

Boswell, R.J., Jessup, S.D., Kim, K.-H. (1981), "Periodic Single-Blade Loads on Propellers in Tangential and Longitudinal Wakes", Propellers '81 Symposium, David W. Taylor Naval Ship Research and Development Center.

Carrica, P.M., Wilson, R.V., Noack, R.W., Stern F. (2007), "Ship motions using single-phase level set with dynamic overset grids," Comput. Fluids 36, 1415-1433.

Chase, N, Carrica, P.M. (2013), "CFD Simulations of a Submarine Propeller and Application to Self-Propulsion of a Submarine," Ocean Eng. 60, 68-80.

Hough, G., Ordway, D. (1965), "The generalized actuator disk", Developments in Theoretical and Applied Mechanics, 2, 317-336.

Kerwin, J.E., Kinnas, S.A., Lee, J.-T., Shih, W.-Z. (1987), "A Surface Panel Method for the Hydrodynamic Analysis of Ducted Propellers", Trans. Soc. Naval Arch. and Marine Eng., 95, 93-122.

Martin, J.E., Michael, T., Carrica, P.M. (2014), "Overset Simulations of a Submarine in Self-Propelled and Maneuvering Conditions", 30th Symposium on Naval Hydrodynamics, Hobart, Australia.

Menter FR, (1994), "2-equation Eddy Viscosity Turbulence Models per Engineering Applications," AIAA J. 32, 1598-1605.

Warren, C. L., Taylor, T.E., Kerwin, J.E. (2000), "A Coupled Viscous/Potential-Flow Method for the Prediction of Propeller-Induced Maneuvering Forces," SNAME Propellers/Shafting 2000 Symposium, Virginia Beach, VA.